Channel Measurement for Holographic MIMO: Benefits and Challenges of Spatial Oversampling

Tengjiao Wang*, Yongxi Liu†, Ming Zhang†, Wei E. I. Sha††,
Cen Ling*, Chao Li*, Shaobo Wang*

2023.05.31

*Wireless Network RAN Research Department, Huawei Technologies CO., Ltd, Shanghai, China

†School of Electronic and Information Engineering, Xi'an Jiaotong University, Shaanxi, China

†† College of Information Science and Electronic Engineering, Zhejiang University, Hangzhou, China

Background

- **Holographic MIMO**: By integrating an infinite number of antennas into a limited surface, holographic MIMO is expected to fully exploit the propagation characteristics offered by the electromagnetic channel and approach the fundamental performance limit. [1-2]

- **EM-Compliant Channel Modeling**: One of the key challenges for Holographic MIMO. Many efforts have been devoted to accurately model the channel of holographic MIMO systems. [3-5] In our previous work, an EM-compliant channel model is proposed, which takes the **non-isotropic characteristics of the propagation environment**, the **antenna pattern distortion**, the **antenna efficiency** into consideration.

- **Key Problems**:

1. The **polarization** of EM wave is not taken into consideration.
2. No **experiments** have been done to verify the accuracy of the channel model and the performance evaluations of holographic MIMO.

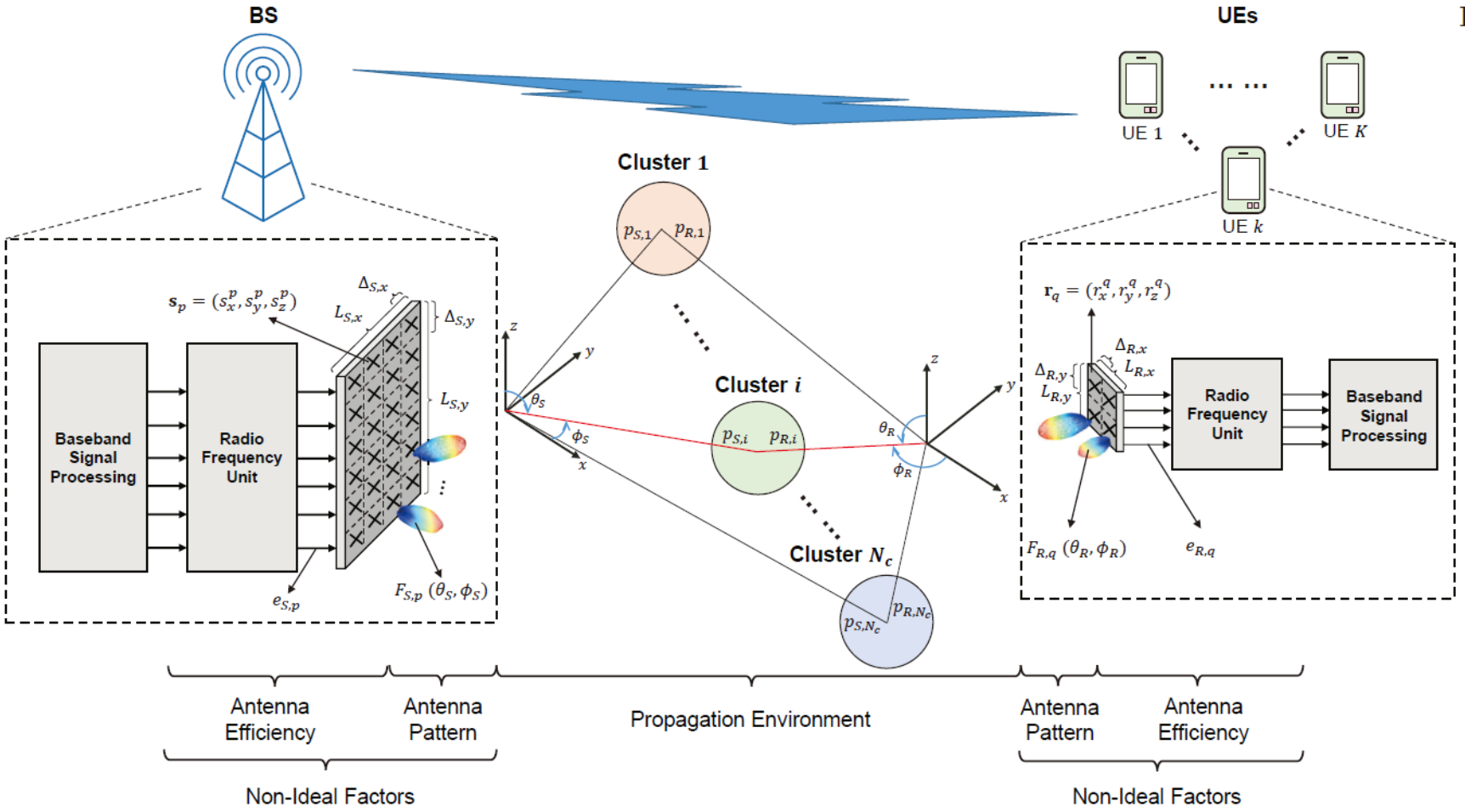
Contributions

- An **EM-compliant channel model** is proposed for holographic MIMO systems. In the proposed model, not only the **non-isotropic characteristics of the propagation environment**, the **antenna pattern distortion**, the **antenna efficiency**, but also the **polarization** of the antennas and the propagation environment can be modeled.

- The **real-world channel for holographic MIMO systems is measured for the first time** in an indoor environment. An experiment is carefully designed, in which an electrically controlled virtual dense array is used to realize arbitrary element spacings of holographic MIMO.

- The channel capacity of holographic MIMO systems is evaluated according to the measurement results. It is demonstrated that the spatial oversampling of holographic MIMO is able to provide a **two to three times capacity enhancement, without considering the antenna efficiency loss**. The **antenna efficiency** is the most crucial challenge for holographic MIMO.

EM-Compliant Channel Model – Previous Work [6]



Channel matrix

$$\mathbf{H} = \sqrt{N_{\mathrm{R}} N_{\mathrm{S}}} \times \sum_{l_x, l_y} \sum_{m_x, m_y} H_{\mathrm{a}}(l_x, l_y, m_x, m_y) \mathbf{a}_{\mathrm{R}}(l_x, l_y) \mathbf{a}_{\mathrm{S}}^{\mathrm{H}}(m_x, m_y),$$

Phase-shifted 2D Fourier harmonics

$$[\mathbf{a}_{\mathrm{S}}(m_x, m_y)]_p = \frac{1}{\sqrt{N_{\mathrm{S}}}} e^{-j\left(\frac{2\pi m_x}{L_{\mathrm{S},x}} s_x^p + \frac{2\pi m_y}{L_{\mathrm{S},y}} s_y^p + \gamma_{\mathrm{S}}(m_x, m_y) s_z^p\right)},$$

$$[\mathbf{a}_{\mathrm{R}}(l_x, l_y)]_q = \frac{1}{\sqrt{N_{\mathrm{R}}}} e^{j\left(\frac{2\pi l_x}{L_{\mathrm{R},x}} r_x^q + \frac{2\pi l_y}{L_{\mathrm{R},y}} r_y^q + \gamma_{\mathrm{R}}(l_x, l_y) r_z^q\right)}$$

Random Fourier coefficient

$$H_{\mathrm{a}}(l_x, l_y, m_x, m_y) \sim \mathcal{CN}(\sigma^2(l_x, l_y, m_x, m_y))$$

$$\sigma^2(l_x, l_y, m_x, m_y) = \iint_{\Omega_{\mathrm{R}}(l_x, l_y)} A^2(\theta_{\mathrm{R}}, \phi_{\mathrm{R}}) \sin\theta_{\mathrm{R}} \mathrm{d}\theta_{\mathrm{R}} \mathrm{d}\phi_{\mathrm{R}} \times \iint_{\Omega_{\mathrm{S}}(m_x, m_y)} A^2(\theta_{\mathrm{S}}, \phi_{\mathrm{S}}) \sin\theta_{\mathrm{S}} \mathrm{d}\theta_{\mathrm{S}} \mathrm{d}\phi_{\mathrm{S}},$$

Matrix Form

$$\mathbf{H} = \mathbf{U}_{\mathrm{R}} \mathbf{H}_{\mathrm{a}} \mathbf{U}_{\mathrm{S}}^{\mathrm{H}}$$

[6] T. Wang, W. Han, Z. Zhong, J. Pang, G. Zhou, S. Wang, and Q. Li, "Electromagnetic-compliant channel modeling and performance evaluation for holographic MIMO," in *IEEE Global Communications Conference (GLOBECOM)*, Rio de Janeiro, Brazil, Dec. 2022.

EM-Compliant Channel Model – Angular Power Spectrum

Mises-Fisher (VMF) distributions [8]

Angular power spectrum

$$A_{\mathrm{S}}^2(\theta_{\mathrm{S}},\phi_{\mathrm{S}}) = \sum_{i=1}^{N_c} w_{\mathrm{S},i} p_{\mathrm{S},i}(\theta_{\mathrm{S}},\phi_{\mathrm{S}})$$

$$A_{\mathrm{R}}^2(\theta_{\mathrm{R}},\phi_{\mathrm{R}}) = \sum_{i=1}^{N_c} w_{\mathrm{R},i} p_{\mathrm{R},i}(\theta_{\mathrm{R}},\phi_{\mathrm{R}})$$

PDF of 3D VMF distribution

$$p_{\mathrm{S},i}(\theta_{\mathrm{S}},\phi_{\mathrm{S}}) = \frac{\alpha_{\mathrm{S},i}}{4\pi\sinh(\alpha_{\mathrm{S},i})} \times e^{\alpha_{\mathrm{S},i}(\sin\theta_{\mathrm{S}}\sin\bar{\theta}_{\mathrm{S},i}\cos(\phi_{\mathrm{S}}-\bar{\phi}_{\mathrm{S},i})+\cos\theta_{\mathrm{S}}\cos\bar{\theta}_{\mathrm{S},i})}$$

$$p_{\mathrm{R},i}(\theta_{\mathrm{R}},\phi_{\mathrm{R}}) = \frac{\alpha_{\mathrm{R},i}}{4\pi\sinh(\alpha_{\mathrm{R},i})} \times e^{\alpha_{\mathrm{R},i}(\sin\theta_{\mathrm{R}}\sin\bar{\theta}_{\mathrm{R},i}\cos(\phi_{\mathrm{R}}-\bar{\phi}_{\mathrm{R},i})+\cos\theta_{\mathrm{R}}\cos\bar{\theta}_{\mathrm{R},i})}$$

Normalization factor

$$\sum_i^{N_c} w_{\mathrm{S},i} = \sum_i^{N_c} w_{\mathrm{R},i} = 1$$

3GPP TR 38.901 [9]

Cluster delay line (CDL)

$$\bar{\phi}_{\mathrm{S},i} = \phi_{i,\mathrm{AoD}} \qquad \bar{\theta}_{\mathrm{S},i} = \theta_{i,\mathrm{ZoD}}$$

$$\bar{\phi}_{\mathrm{R},i} = \phi_{i,\mathrm{AoA}} \qquad \bar{\theta}_{\mathrm{R},i} = \theta_{i,\mathrm{ZoA}}$$

*Table 7.7.1-2 in [9]

Concentration parameter

$$\alpha_{\mathrm{S},i} = \frac{212.9^2}{\delta_{\mathrm{ASD}}^2}, \quad \alpha_{\mathrm{R},i} = \frac{212.9^2}{\delta_{\mathrm{ASA}}^2}$$

*Appendix 3.1 in [13]

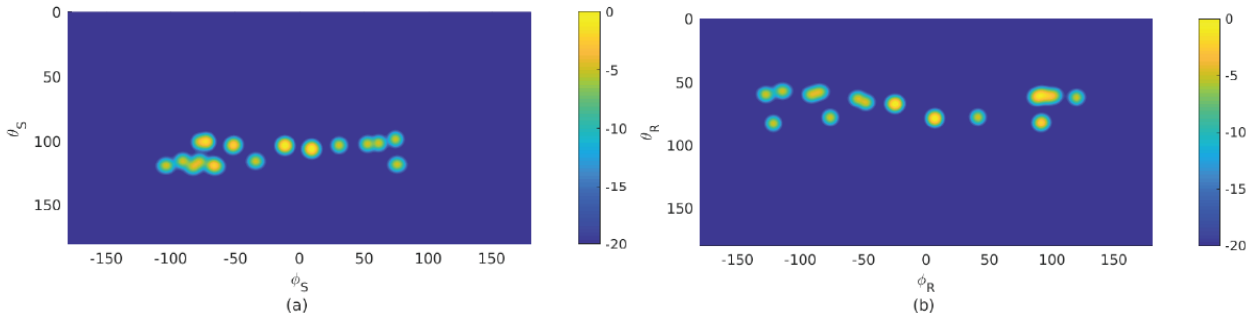


Illustration of the anglular power spectrum of the propagation channel based on 3GPP CDL-B channel model. a) Anglular power spectrum at BS; b) Anglular power spectrum at UE..

EM-Compliant Channel Model – Antenna Pattern Distortion

- Firstly, the **distorted antenna pattern** will be different from that of an **isolated element**.
- Secondly, the distorted antenna patterns of **different elements** will also be different based on the **locations** of the elements in the array

Normalized embedded antenna pattern

$$F_{\mathrm{S},p}(\theta_{\mathrm{S}},\phi_{\mathrm{S}}) \qquad F_{\mathrm{R},q}(\theta_{\mathrm{R}},\phi_{\mathrm{R}})$$

Modified Fourier harmonic

$$[\boldsymbol{\psi}_{\mathrm{S}}(m_x,m_y)]_p = \frac{1}{\sqrt{N_{\mathrm{S}}}} e^{-j\left(\frac{2\pi m_x}{L_{\mathrm{S},x}} s_x^p + \frac{2\pi m_y}{L_{\mathrm{S},y}} s_y^p + \gamma_{\mathrm{S}}(m_x,m_y) s_z^p\right)} \times F_{\mathrm{S},p}\left(\theta_{\mathrm{S}}^*(m_x,m_y), \phi_{\mathrm{S}}^*(m_x,m_y)\right),$$

$$[\boldsymbol{\psi}_{\mathrm{R}}(l_x,l_y)]_q = \frac{1}{\sqrt{N_{\mathrm{R}}}} e^{j\left(\frac{2\pi l_x}{L_{\mathrm{R},x}} r_x^q + \frac{2\pi l_y}{L_{\mathrm{R},y}} r_y^q + \gamma_{\mathrm{R}}(l_x,l_y) r_z^q\right)} \times F_{\mathrm{R},q}\left(\theta_{\mathrm{R}}^*(l_x,l_y), \phi_{\mathrm{R}}^*(l_x,l_y)\right),$$

Elevation angle

$$\theta_{\mathrm{S}}^*(m_x,m_y) = \arccos\left(\sqrt{1-\left(\frac{m_x\lambda}{L_{\mathrm{S},x}}\right)^2 - \left(\frac{m_y\lambda}{L_{\mathrm{S},y}}\right)^2}\right)$$

$$\theta_{\mathrm{R}}^*(l_x,l_y) = \arccos\left(\sqrt{1-\left(\frac{l_x\lambda}{L_{\mathrm{R},x}}\right)^2 - \left(\frac{l_y\lambda}{L_{\mathrm{R},y}}\right)^2}\right)$$

Azimuth angle

$$\phi_{\mathrm{S}}^*(m_x,m_y) = \arctan\left(\frac{L_{\mathrm{S},x} m_y}{L_{\mathrm{S},y} m_x}\right)$$

$$\phi_{\mathrm{R}}^*(l_x,l_y) = \arctan\left(\frac{L_{\mathrm{R},x} l_y}{L_{\mathrm{R},y} l_x}\right)$$

Overall Channel Matrix

$$\mathbf{H} = \boldsymbol{\Psi}_{\mathrm{R}} \mathbf{H}_{\mathrm{a}} \boldsymbol{\Psi}_{\mathrm{S}}^{\mathrm{H}}$$

EM-Compliant Channel Model – Antenna Efficiency

- In a dense antenna array with small element spacing, the efficiency of the antenna elements will be decreased because of the **mutual coupling** among them.
- The reason is that due to the effect of **mutual coupling**, the **active impedance** of each element varies with **scan angles**. The **impedance mismatch** between the antenna elements and the transmission lines causes the power to be returned to the generators.

Antenna Efficiency

$$e_{\mathrm{S},p} = 1 - \sum_{p'=1}^{N_\mathrm{S}} \|[\mathbf{S}_\mathrm{S}]_{p,p'}\|^2,$$

$$e_{\mathrm{R},q} = 1 - \sum_{q'=1}^{N_\mathrm{R}} \|[\mathbf{S}_\mathrm{R}]_{q,q'}\|^2,$$

Hannan's Efficiency [12]

$$e^*_{\mathrm{S},p}(\Delta_{\mathrm{S},x}, \Delta_{\mathrm{S},y}) = \frac{\pi L_{\mathrm{S},x} L_{\mathrm{S},y}}{N_\mathrm{S}\lambda^2} = \frac{\pi \Delta_{\mathrm{S},x} \Delta_{\mathrm{S},y}}{\lambda^2}$$

$$e^*_{\mathrm{R},q}(\Delta_{\mathrm{R},x}, \Delta_{\mathrm{R},y}) = \frac{\pi L_{\mathrm{R},x} L_{\mathrm{R},y}}{N_\mathrm{R}\lambda^2} = \frac{\pi \Delta_{\mathrm{R},x} \Delta_{\mathrm{R},y}}{\lambda^2}$$

Relative Efficiency

$$\eta_{\mathrm{S},p} = \frac{e_{\mathrm{S},p}}{e^*_{\mathrm{S},p}(\frac{\lambda}{2}, \frac{\lambda}{2})}$$

$$\eta_{\mathrm{R},q} = \frac{e_{\mathrm{R},q}}{e^*_{\mathrm{R},q}(\frac{\lambda}{2}, \frac{\lambda}{2})}.$$

Overall Channel Matrix

$$\mathbf{H} = \mathbf{\Gamma}_\mathrm{R} \mathbf{\Psi}_\mathrm{R} \mathbf{H}_\mathrm{a} \mathbf{\Psi}_\mathrm{S}^\mathrm{H} \mathbf{\Gamma}_\mathrm{S}$$

EM-Compliant Channel Model – Polarization

- According to [10], the **polarization pattern** of an EM wave can be decomposed into **two components orthogonal to the propagation direction**, i.e., the **vertical polarization** and the **horizontal polarization**.
- Therefore, the channel considering the polarization characteristics can be written as

Single-Polarization

$$[\mathbf{H}]_{q,p} = \sum_{\beta=1}^{n_{\mathrm{R}}} \sum_{\alpha=1}^{n_{\mathrm{S}}} \eta_{\mathrm{R},q} [\mathbf{\Psi}_{\mathrm{R}}]_{q,\beta} [\mathbf{H}_{\mathrm{a}}]_{\beta,\alpha} [\mathbf{\Psi}_{\mathrm{S}}]^*_{p,\alpha} \eta_{\mathrm{S},p}$$

Dual-Polarization

$$\begin{aligned}
[\mathbf{H}]^{\mathrm{pol}}_{q,p} = & \sum_{\beta=1}^{n_{\mathrm{R}}} \sum_{\alpha=1}^{n_{\mathrm{S}}} \eta_{\mathrm{R},q} [\mathbf{\Psi}^{\theta}_{\mathrm{R}}]_{q,\beta} [\mathbf{H}^{\theta\theta}_{\mathrm{a}}]_{\beta,\alpha} [\mathbf{\Psi}^{\theta}_{\mathrm{S}}]^*_{p,\alpha} \eta_{\mathrm{S},p} \\
& + \sum_{\beta=1}^{n_{\mathrm{R}}} \sum_{\alpha=1}^{n_{\mathrm{S}}} \eta_{\mathrm{R},q} [\mathbf{\Psi}^{\theta}_{\mathrm{R}}]_{q,\beta} [\mathbf{H}^{\theta\phi}_{\mathrm{a}}]_{\beta,\alpha} [\mathbf{\Psi}^{\phi}_{\mathrm{S}}]^*_{p,\alpha} \eta_{\mathrm{S},p} \\
& + \sum_{\beta=1}^{n_{\mathrm{R}}} \sum_{\alpha=1}^{n_{\mathrm{S}}} \eta_{\mathrm{R},q} [\mathbf{\Psi}^{\phi}_{\mathrm{R}}]_{q,\beta} [\mathbf{H}^{\phi\theta}_{\mathrm{a}}]_{\beta,\alpha} [\mathbf{\Psi}^{\theta}_{\mathrm{S}}]^*_{p,\alpha} \eta_{\mathrm{S},p} \\
& + \sum_{\beta=1}^{n_{\mathrm{R}}} \sum_{\alpha=1}^{n_{\mathrm{S}}} \eta_{\mathrm{R},q} [\mathbf{\Psi}^{\phi}_{\mathrm{R}}]_{q,\beta} [\mathbf{H}^{\phi\phi}_{\mathrm{a}}]_{\beta,\alpha} [\mathbf{\Psi}^{\phi}_{\mathrm{S}}]^*_{p,\alpha} \eta_{\mathrm{S},p},
\end{aligned}$$

Polarization of Antennas

	UE	BS
θ	$[\mathbf{\Psi}^{\theta}_{\mathrm{R}}]_{q,\beta} = \frac{1}{\sqrt{N_{\mathrm{R}}}} e^{j\left(\frac{2\pi l^x_\beta}{L^x_{\mathrm{R}}} r^x_q + \frac{2\pi l^y_\beta}{L^y_{\mathrm{R}}} r^y_q + \gamma_{\mathrm{R}}(l^x_\beta, l^y_\beta) r^z_q\right)} \times F^{\theta}_{\mathrm{R},q}\left(\hat{\theta}_{\mathrm{R}}(l^x_\beta, l^y_\beta), \hat{\phi}_{\mathrm{R}}(l^x_\beta, l^y_\beta)\right),$	$[\mathbf{\Psi}^{\theta}_{\mathrm{S}}]_{p,\alpha} = \frac{1}{\sqrt{N_{\mathrm{S}}}} e^{j\left(\frac{2\pi m^x_\alpha}{L^x_{\mathrm{S}}} s^x_p + \frac{2\pi m^y_\alpha}{L^y_{\mathrm{S}}} s^y_p + \gamma_{\mathrm{S}}(m^x_\alpha, m^y_\alpha) s^z_p\right)} \times F^{\theta}_{\mathrm{S},p}\left(\hat{\theta}_{\mathrm{S}}(m^x_\alpha, m^y_\alpha), \hat{\phi}_{\mathrm{S}}(m^x_\alpha, m^y_\alpha)\right),$
ϕ	$[\mathbf{\Psi}^{\phi}_{\mathrm{R}}]_{q,\beta} = \frac{1}{\sqrt{N_{\mathrm{R}}}} e^{j\left(\frac{2\pi l^x_\beta}{L^x_{\mathrm{R}}} r^x_q + \frac{2\pi l^y_\beta}{L^y_{\mathrm{R}}} r^y_q + \gamma_{\mathrm{R}}(l^x_\beta, l^y_\beta) r^z_q\right)} \times F^{\phi}_{\mathrm{R},q}\left(\hat{\theta}_{\mathrm{R}}(l^x_\beta, l^y_\beta), \hat{\phi}_{\mathrm{R}}(l^x_\beta, l^y_\beta)\right),$	$[\mathbf{\Psi}^{\phi}_{\mathrm{S}}]_{p,\alpha} = \frac{1}{\sqrt{N_{\mathrm{S}}}} e^{j\left(\frac{2\pi m^x_\alpha}{L^x_{\mathrm{S}}} s^x_p + \frac{2\pi m^y_\alpha}{L^y_{\mathrm{S}}} s^y_p + \gamma_{\mathrm{S}}(m^x_\alpha, m^y_\alpha) s^z_p\right)} \times F^{\phi}_{\mathrm{S},p}\left(\hat{\theta}_{\mathrm{S}}(m^x_\alpha, m^y_\alpha), \hat{\phi}_{\mathrm{S}}(m^x_\alpha, m^y_\alpha)\right),$

Polarization of Propagation Environment

	co-polarization	cross-polarization
$[\mathbf{H}^{\theta\theta}_{\mathrm{a}}]_{\beta,\alpha}$	$= [\mathbf{H}_{\mathrm{a}}]_{\beta,\alpha} \times e^{j\Phi^{\theta\theta}_{\beta,\alpha}},$	$[\mathbf{H}^{\theta\phi}_{\mathrm{a}}]_{\beta,\alpha} = [\mathbf{H}_{\mathrm{a}}]_{\beta,\alpha} \times e^{j\Phi^{\theta\phi}_{\beta,\alpha}} \times \sqrt{\kappa^{-1}_{\beta,\alpha}},$
$[\mathbf{H}^{\phi\phi}_{\mathrm{a}}]_{\beta,\alpha}$	$= [\mathbf{H}_{\mathrm{a}}]_{\beta,\alpha} \times e^{j\Phi^{\phi\phi}_{\beta,\alpha}}.$	$[\mathbf{H}^{\phi\theta}_{\mathrm{a}}]_{\beta,\alpha} = [\mathbf{H}_{\mathrm{a}}]_{\beta,\alpha} \times e^{j\Phi^{\phi\theta}_{\beta,\alpha}} \times \sqrt{\kappa^{-1}_{\beta,\alpha}},$

$\Phi^{\theta\theta}_{\beta,\alpha}$, $\Phi^{\phi\phi}_{\beta,\alpha}$, $\Phi^{\phi\theta}_{\beta,\alpha}$, and $\Phi^{\theta\phi}_{\beta,\alpha}$ random phase shifts, $[-\pi, \pi]$

$\kappa_{\beta,\alpha} = 10^{X_{\beta,\alpha}/10}$: cross polarization power ratios (XPR)

$X_{\beta,\alpha} \sim \mathcal{N}(\mu_{\mathrm{XPR}}, \sigma^2_{\mathrm{XPR}})$

EM-Compliant Channel Model – Polarization

- Finally, we transform the item-wise channel model into a **matrix form**.

Item-wise channel model

$$
\begin{aligned}
[\mathbf{H}]_{q,p}^{\mathrm{pol}} = & \sum_{\beta=1}^{n_{\mathrm{R}}} \sum_{\alpha=1}^{n_{\mathrm{S}}} \eta_{\mathrm{R},q} [\boldsymbol{\Psi}_{\mathrm{R}}^{\theta}]_{q,\beta} [\mathbf{H}_{\mathrm{a}}^{\theta\theta}]_{\beta,\alpha} [\boldsymbol{\Psi}_{\mathrm{S}}^{\theta}]_{p,\alpha}^{*} \eta_{\mathrm{S},p} \\
& + \sum_{\beta=1}^{n_{\mathrm{R}}} \sum_{\alpha=1}^{n_{\mathrm{S}}} \eta_{\mathrm{R},q} [\boldsymbol{\Psi}_{\mathrm{R}}^{\theta}]_{q,\beta} [\mathbf{H}_{\mathrm{a}}^{\theta\phi}]_{\beta,\alpha} [\boldsymbol{\Psi}_{\mathrm{S}}^{\phi}]_{p,\alpha}^{*} \eta_{\mathrm{S},p} \\
& + \sum_{\beta=1}^{n_{\mathrm{R}}} \sum_{\alpha=1}^{n_{\mathrm{S}}} \eta_{\mathrm{R},q} [\boldsymbol{\Psi}_{\mathrm{R}}^{\phi}]_{q,\beta} [\mathbf{H}_{\mathrm{a}}^{\phi\theta}]_{\beta,\alpha} [\boldsymbol{\Psi}_{\mathrm{S}}^{\theta}]_{p,\alpha}^{*} \eta_{\mathrm{S},p} \\
& + \sum_{\beta=1}^{n_{\mathrm{R}}} \sum_{\alpha=1}^{n_{\mathrm{S}}} \eta_{\mathrm{R},q} [\boldsymbol{\Psi}_{\mathrm{R}}^{\phi}]_{q,\beta} [\mathbf{H}_{\mathrm{a}}^{\phi\phi}]_{\beta,\alpha} [\boldsymbol{\Psi}_{\mathrm{S}}^{\phi}]_{p,\alpha}^{*} \eta_{\mathrm{S},p},
\end{aligned}
$$

Matrix-form channel model

$$
\begin{aligned}
\mathbf{H}^{\mathrm{pol}} = & \boldsymbol{\Gamma}_{\mathrm{R}} \boldsymbol{\Psi}_{\mathrm{R}}^{\theta} \mathbf{H}_{\mathrm{a}}^{\theta\theta} \boldsymbol{\Psi}_{\mathrm{S}}^{\theta\,\mathrm{H}} \boldsymbol{\Gamma}_{\mathrm{S}} + \boldsymbol{\Gamma}_{\mathrm{R}} \boldsymbol{\Psi}_{\mathrm{R}}^{\theta} \mathbf{H}_{\mathrm{a}}^{\theta\phi} \boldsymbol{\Psi}_{\mathrm{S}}^{\phi\,\mathrm{H}} \boldsymbol{\Gamma}_{\mathrm{S}} \\
& + \boldsymbol{\Gamma}_{\mathrm{R}} \boldsymbol{\Psi}_{\mathrm{R}}^{\phi} \mathbf{H}_{\mathrm{a}}^{\phi\theta} \boldsymbol{\Psi}_{\mathrm{S}}^{\theta\,\mathrm{H}} \boldsymbol{\Gamma}_{\mathrm{S}} + \boldsymbol{\Gamma}_{\mathrm{R}} \boldsymbol{\Psi}_{\mathrm{R}}^{\phi} \mathbf{H}_{\mathrm{a}}^{\phi\phi} \boldsymbol{\Psi}_{\mathrm{S}}^{\phi\,\mathrm{H}} \boldsymbol{\Gamma}_{\mathrm{S}} \\
= & \boldsymbol{\Gamma}_{\mathrm{R}} \left[\boldsymbol{\Psi}_{\mathrm{R}}^{\theta}, \boldsymbol{\Psi}_{\mathrm{R}}^{\phi} \right] \begin{bmatrix} \mathbf{H}_{\mathrm{a}}^{\theta\theta} & \mathbf{H}_{\mathrm{a}}^{\theta\phi} \\ \mathbf{H}_{\mathrm{a}}^{\phi\theta} & \mathbf{H}_{\mathrm{a}}^{\phi\phi} \end{bmatrix} \left[\boldsymbol{\Psi}_{\mathrm{S}}^{\theta}, \boldsymbol{\Psi}_{\mathrm{S}}^{\phi} \right]^{\mathrm{H}} \boldsymbol{\Gamma}_{\mathrm{S}}.
\end{aligned}
$$

Final Channel Matrix

$$
\mathbf{H}^{\mathrm{pol}} = \boldsymbol{\Gamma}_{\mathrm{R}} \boldsymbol{\Psi}_{\mathrm{R}}^{\mathrm{pol}} \mathbf{H}_{\mathrm{a}}^{\mathrm{pol}} \boldsymbol{\Psi}_{\mathrm{S}}^{\mathrm{pol}\,\mathrm{H}} \boldsymbol{\Gamma}_{\mathrm{S}}
$$

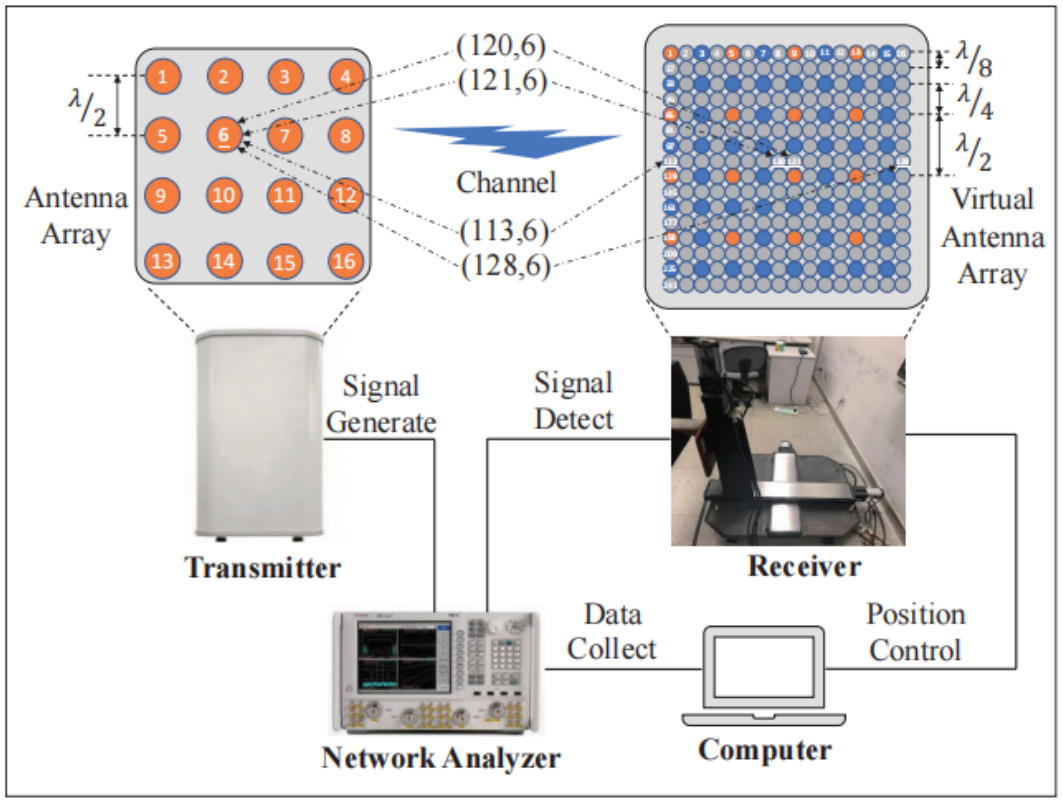
$$
\boldsymbol{\Psi}_{\mathrm{R}}^{\mathrm{pol}} = \left[\boldsymbol{\Psi}_{\mathrm{R}}^{\theta}, \boldsymbol{\Psi}_{\mathrm{R}}^{\phi} \right] \qquad \boldsymbol{\Psi}_{\mathrm{S}}^{\mathrm{pol}} = \left[\boldsymbol{\Psi}_{\mathrm{S}}^{\theta}, \boldsymbol{\Psi}_{\mathrm{S}}^{\phi} \right]
$$

$$
\mathbf{H}_{\mathrm{a}}^{\mathrm{pol}} = \begin{bmatrix} \mathbf{H}_{\mathrm{a}}^{\theta\theta} & \mathbf{H}_{\mathrm{a}}^{\theta\phi} \\ \mathbf{H}_{\mathrm{a}}^{\phi\theta} & \mathbf{H}_{\mathrm{a}}^{\phi\phi} \end{bmatrix}
$$

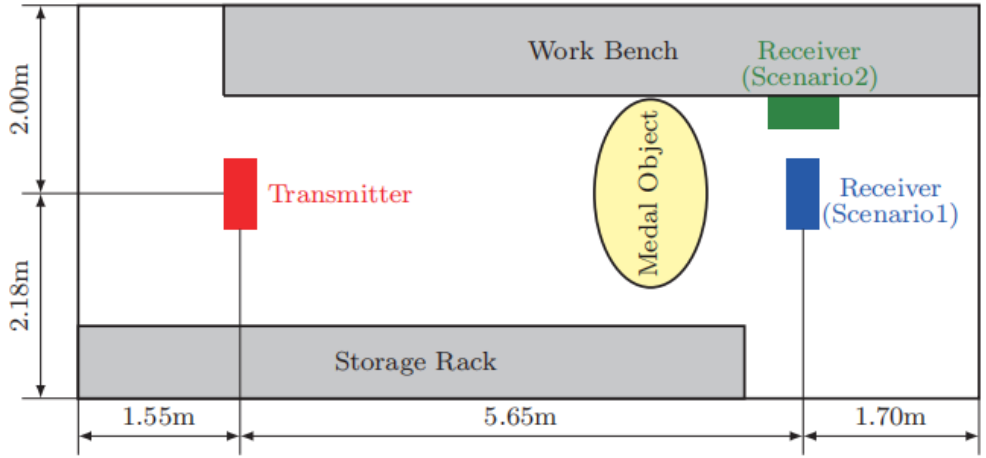
Channel Measurement for Holographic MIMO

- In order to evaluate the EM-compliant channel model and implement a realistic performance evaluation for holographic MIMO systems, an experiment is conducted to **measure the real-world channel** of holographic MIMO systems.

Schematic diagram of the measurement equipment



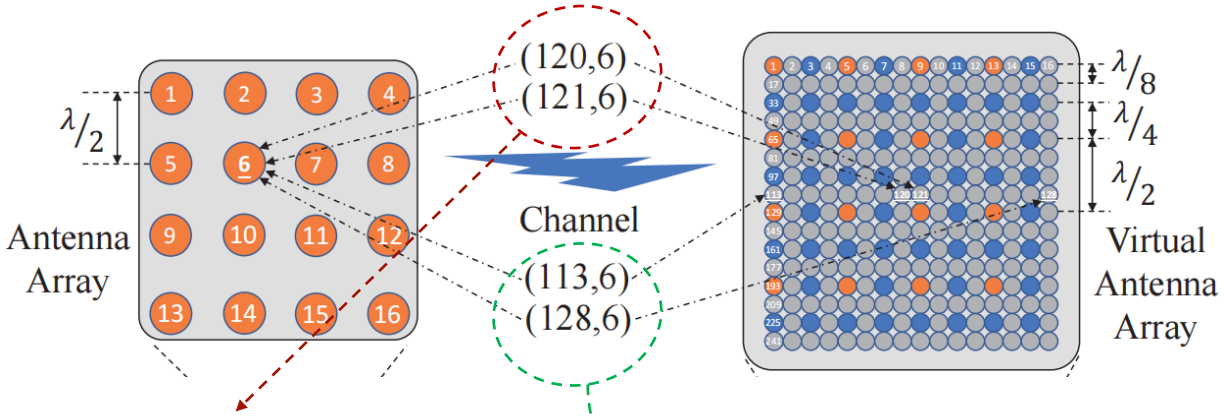
Schematic diagram of the measurement environment

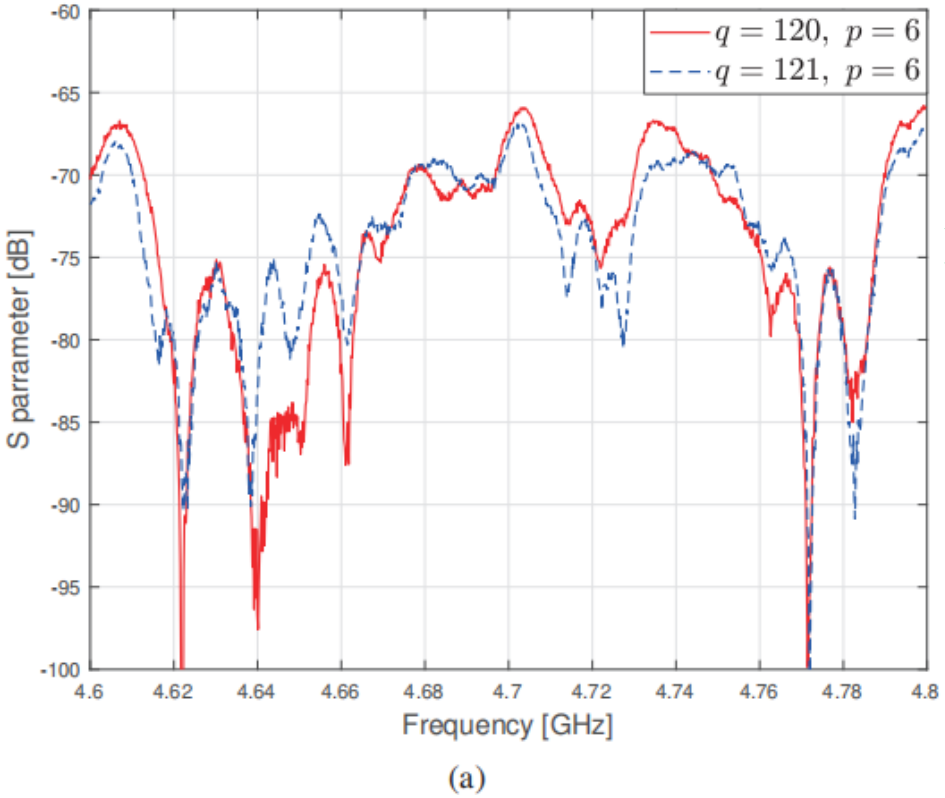


- **Central frequency:** 4.7 GHz
- **Bandwidth:** 200 MHz
- **Transmitter:** 16 Antennas with $\lambda/2$ spacing
- **Receiver:** $\{16,\ 64,\ 256\}$ Antennas with $\{\lambda/2, \lambda/4,\ \lambda/8\}$ spacings

Measurement Results – Channel Response

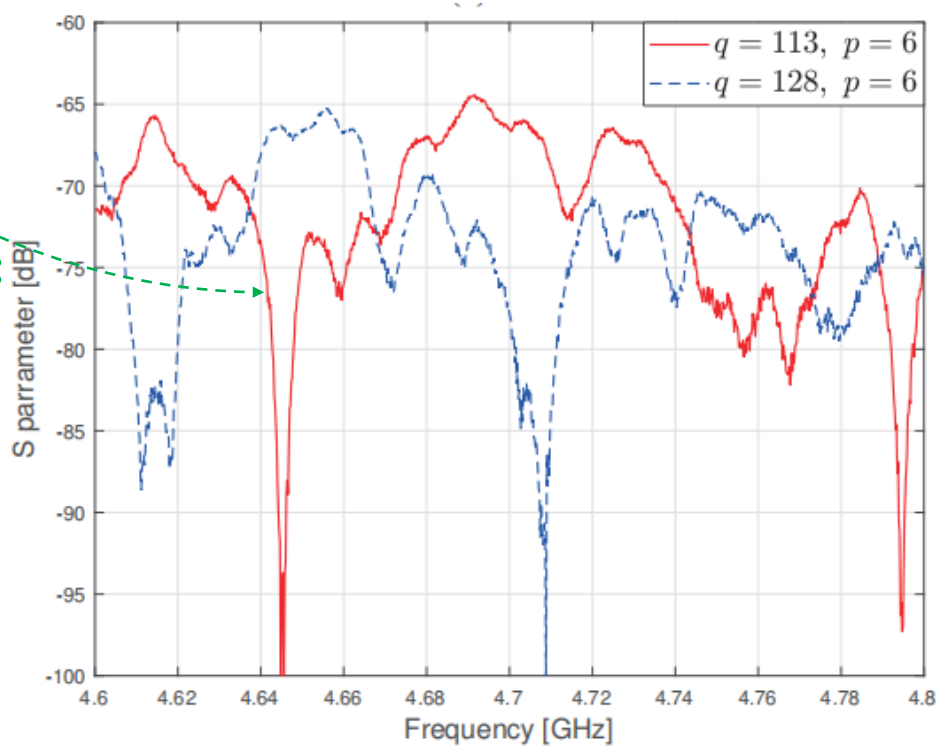
Adjacent element: Similar Channel Responses





(a)

Non-Adjacent element: Different Channel Responses

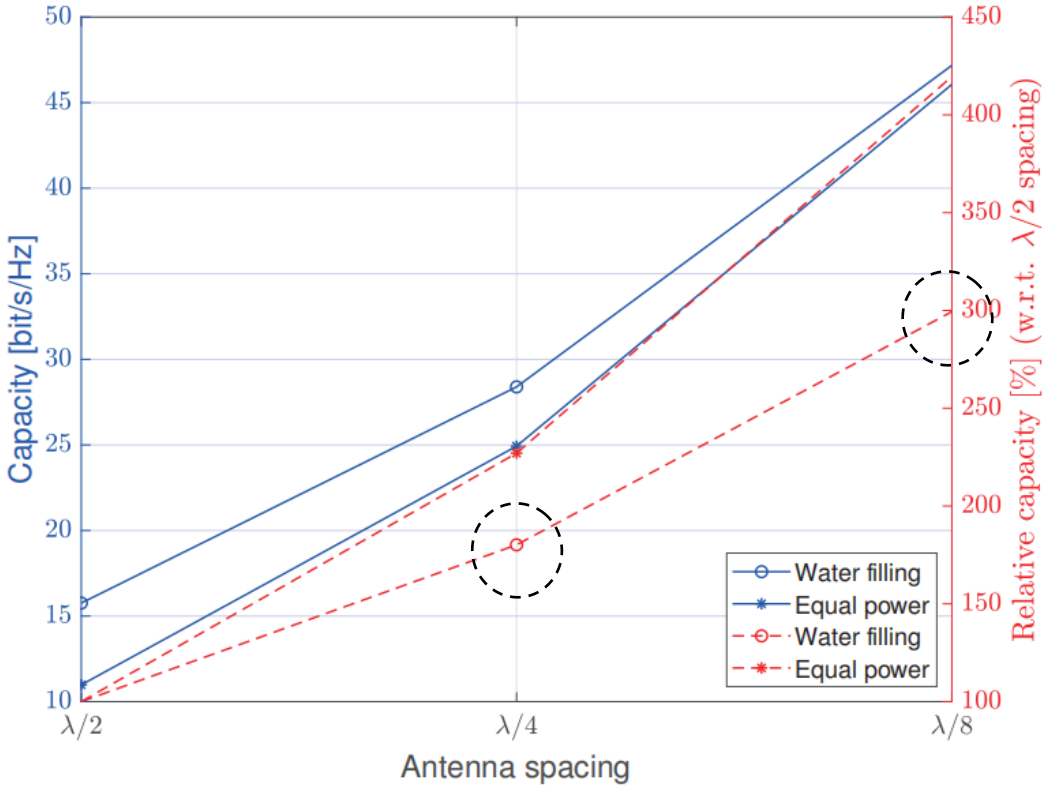


(b)

Measurement Results – Capacity without efficiency loss

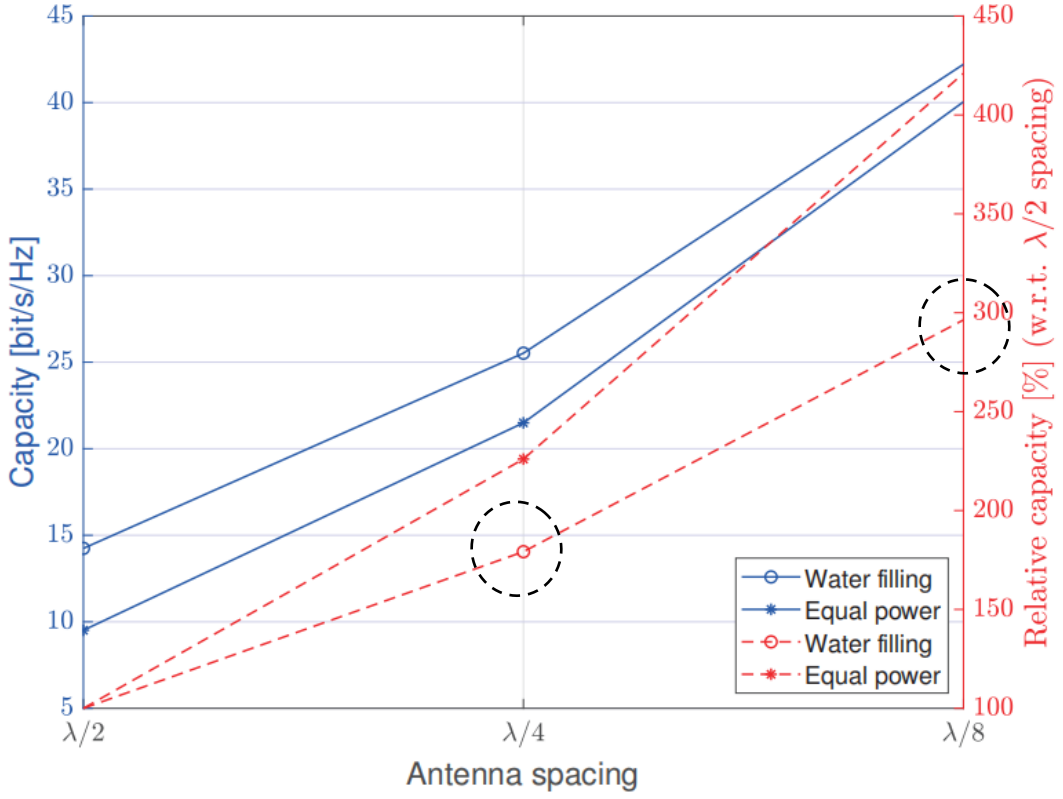
- When the **efficiency loss** of antenna element is **not taken into consideration**, spatial oversampling of holographic MIMO is able to **increase the channel capacity**.
- When using water filling strategy, **$\lambda/4$ oversampling** can offer about **80% capacity gain**, and **$\lambda/8$ oversampling** can offer about **200% capacity gain**.

Scenario 1



(a)

Scenario 2



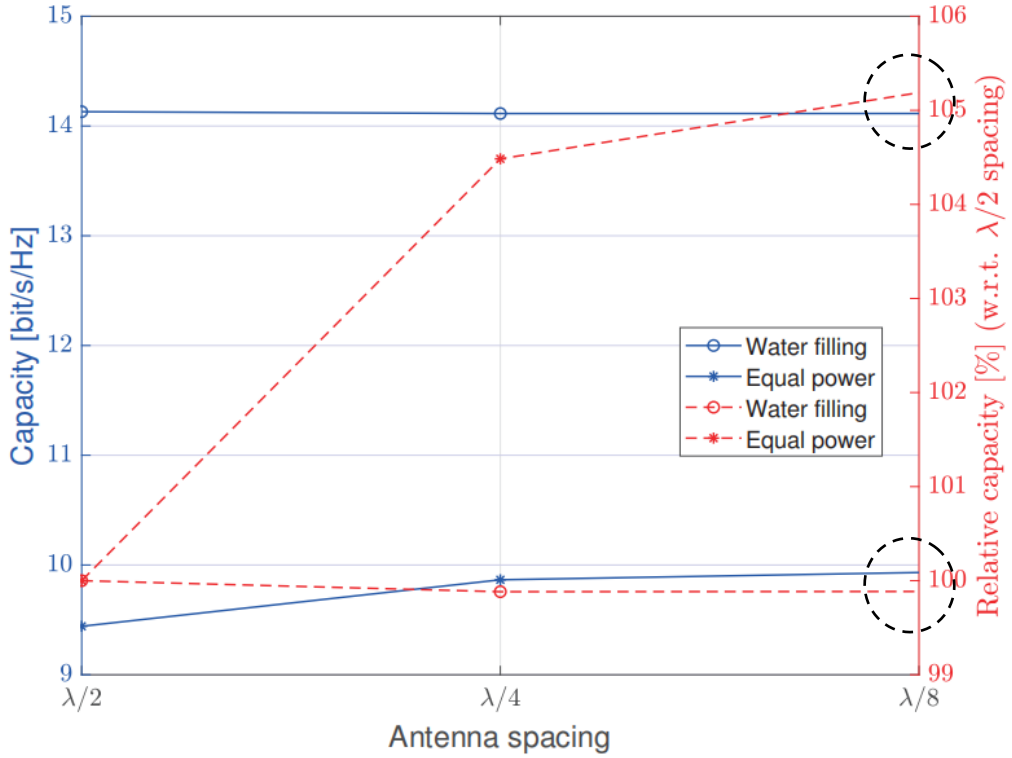
(b)

* SNR = 0 dB

Measurement Results – Capacity with efficiency loss

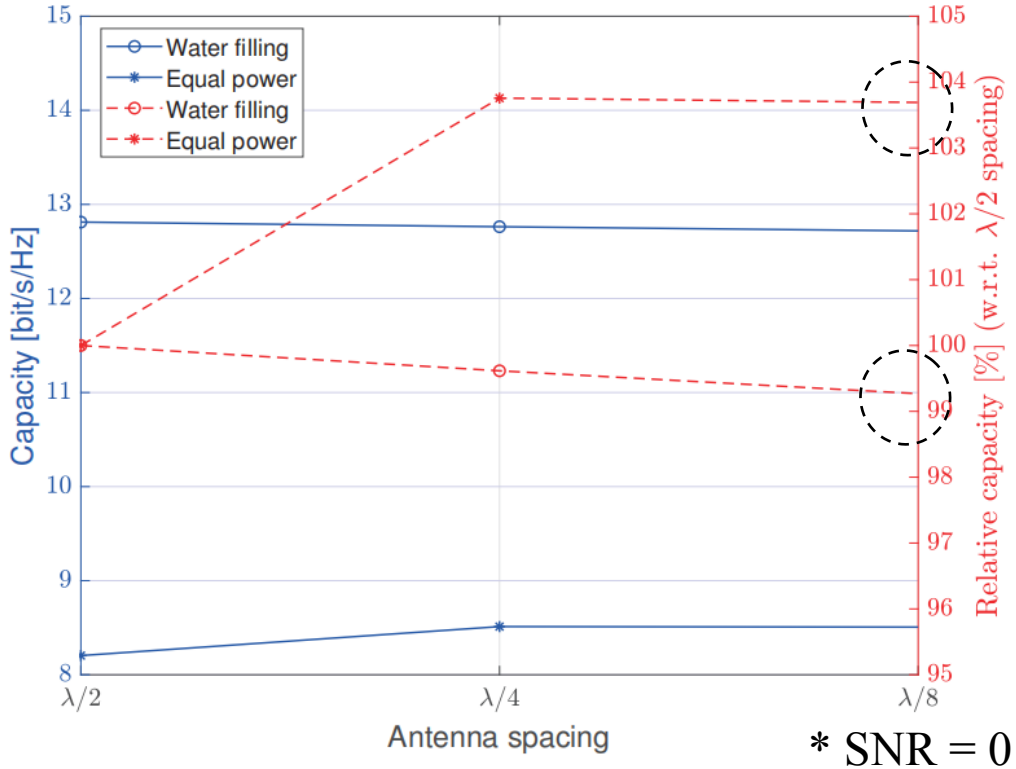
- In a practical dense antenna array with small element spacing, the **efficiency** of the antenna elements will decrease because of the **mutual coupling** among them.
- According to [12], for a practical dense array at the receiver, the efficiency of the antenna element can be estimated as $\eta = \pi \Delta^x \Delta^y / \lambda^2$. (**Hannan's element efficiency**)
- Using **equal power allocation** strategy, it can only provide **4% capacity gain**. While using **water filling strategy**, the capacity even **slightly decrease**.

Scenario 1



(a)

Scenario 2



(b)

* SNR = 0 dB

Summary

Contributions:

1. An **EM-compliant channel model** is proposed for the holographic MIMO systems which has intuitive physical meaning and is more consistent with the realistic environment.
2. An **experiment** is conducted to **measure the channel** of an indoor holographic MIMO system through **virtual antenna arrays**.
3. The **channel capacity** of holographic MIMO systems is evaluated according to the measurement results.

Main Findings:

1. The **spatial oversampling** of holographic MIMO is able to **increase the capacity** of a wireless communication system significantly.
2. However, the **antenna efficiency** is the most crucial challenge preventing us from getting the capacity improvement.

Reference

- [1] C. Huang, S. Hu, G. C. Alexandropoulos, A. Zappone, C. Yuen, R. Zhang, M. D. Renzo, and M. Debbah, "Holographic MIMO surfaces for 6G wireless networks: Opportunities, challenges, and trends," *IEEE Wireless Commun.*, vol. 27, no. 5, pp. 118–125, Oct. 2020.
- [2] D. Dardari and N. Decarli, "Holographic communication using intelligent surfaces," *IEEE Commun. Mag.*, vol. 59, no. 6, pp. 35–41, Jun. 2021.
- [3] A. Pizzo, T. L. Marzetta, and L. Sanguinetti, "Spatially-stationary model for holographic MIMO small-scale fading," *IEEE J. Sel. Areas Commun.*, vol. 38, no. 9, pp. 1964–1979, Sep. 2020.
- [4] L. Wei, C. Huang, G. Alexandropoulus, W. E. I. Sha, Z. Zhang, M. Debbah, and C. Yuen, "Multi-user holographic MIMO surfaces: Channel modeling and spectral effificiency analysis," *IEEE J. Sel. Topics Signal Process.*, vol. 16, no. 5, pp. 1112–1124, Aug. 2022.
- [5] A. Pizzo, L. Sanguinetti, and T. L. Marzetta, "Fourier plane-wave series expansion for holographic MIMO communications," *IEEE Trans. Wireless Commun.*, vol. 21, no. 9, pp. 6890–6905, Sep. 2022.
- [6] T. Wang, W. Han, Z. Zhong, J. Pang, G. Zhou, S. Wang, and Q. Li, "Electromagnetic-compliant channel modeling and performance evaluation for holographic MIMO," in *IEEE Global Communications Conference (GLOBECOM)*, Rio de Janeiro, Brazil, Dec. 2022.
- [7] Y. Liu, M. Zhang, and T. Wang, "Effect of antenna pattern on electromagnetic MIMO communication," in *IEEE International Conference on Communication Technology (ICCT)*, Nanjing, China, Nov. 2022.
- [8] K. Mammasis, R. W. Stewart, and J. S. Thompson, "Spatial fading correlation model using mixtures of von Mises Fisher distributions," *IEEE Trans. Wireless Commun.*, vol. 8, no. 4, pp. 2046–2055, Apr. 2009.
- [9] 3GPP TR 38.901, "Study on channel model for frequencies from 0.5 to 100 GHz," 2020.
- [10] C. A. Balanis, *Antenna Theory: Analysis and Design*. New York: John Wiley & Sons Ltd, 2015.
- [11] Z. Zhang and L. Dai, "Continuous-aperture MIMO for electromagnetic information theory," arXiv, 2021. [Online].
- [12] P. Hannan, "The element-gain paradox for a phased-array antenna," *IEEE Trans. Antenna Propag.*, vol. 12, no. 4, pp. 423–433, Jul. 1964.
- [13] K. V. Mardia and P. E. Jupp, Directional Statistics. New York: John Wiley & Sons Ltd, 2000.

Thank You